Numerical and Experimental study of elementary interactions in marine current turbines array

Clément Carlier, Grégory Pinon, Benoît Gaurier, Grégory Germain, Elie Rivoalen

Numerical and Experimental study of elementary interactions in marine current turbines array

Clément Carlier*†, Grégory Pinon*, Benoît Gaurier†, Grégory Germain† and Élie Rivoalen*§
*Laboratoire Ondes et Milieux Complexes (LOMC), UMR 6294, CNRS – Université du Havre,
E-mail: gregory.pinon@univ-lehavre.fr
†IFREMER, Marine Structures Laboratory
E-mails: {clement.carlier, benoit.gaurier, gregory.germain}@ifremer.fr
§Laboratoire d'Optimisation et Fiabilité en Mécanique des Structures (LOFIMS), EA 3828, INSA de Rouen,
E-mail: elie.rivoalen@insa-rouen.fr

***Abstract*—The development of marine current turbines arrays has been an active research topic for some years. However, many studies are still necessary in order to fully understand the behaviour of such arrays. One of these studies is the assessment of interaction effect between turbines in close proximity. In order to highlight these interaction effects, experiments were carried out in the IFREMER flume tank of Boulogne-Sur-Mer (France). Those experiments focused on elementary interactions between two or three 3-bladed horizontal axis turbines. To complete these experiments, a three-dimensional software is developed at LOMC (Université du Havre) to simulate marine current turbines in a free flow. This paper presents the experimental and numerical results obtained for different configurations of elementary interactions.**

***Index Terms*—Marine current turbine, Interacting turbines, Experiment, Numerical computations, Wake, Performance.**

I. Introduction

The development of marine current turbines arrays has been an active research topic for some years [1]–[5]. However, many studies are still necessary in order to fully understand the behaviour of such arrays. One of these studies is the assessment of interaction effect between turbines in close proximity. In order to describe those effects, the study of three cases of elementary interactions is proposed. The three configurations are described in red, green and blue in Fig. 1.

The first configuration (red in Fig. 1), representing the one studied by Mycek *et al.* [4], is composed of two turbines aligned with the upstream flow. The second (green in Fig. 1) and third one (blue in Fig. 1) were already experimentally studied by, among others, Kervella *et al.* [5]. These two last configurations are composed of two rows of turbines, one with a single turbine and the other one composed two turbines. The only difference between the second and third configuration is the order of those two rows of machines.

The first part of this paper is dedicated to the presentation of the numerical method used to compute the flow around three bladed horizontal axis marine current turbines. Some new features were recently implemented in the software in order to speed up the calculation for multi-turbines configurations. This consists of an iterative method to the solve the linear system representing interaction between turbines. Additionally, a well suited preconditioner was added to obtain an accurate and computationally efficient numerical model. Then in a second part, experimental results of interactions between two aligned turbines are given. The third part of this paper is dedicated to numerical results obtained for the three configurations of elementary interactions presented here. Eventually, conclusions are drawn and an outlook on future numerical and experimental works is given.

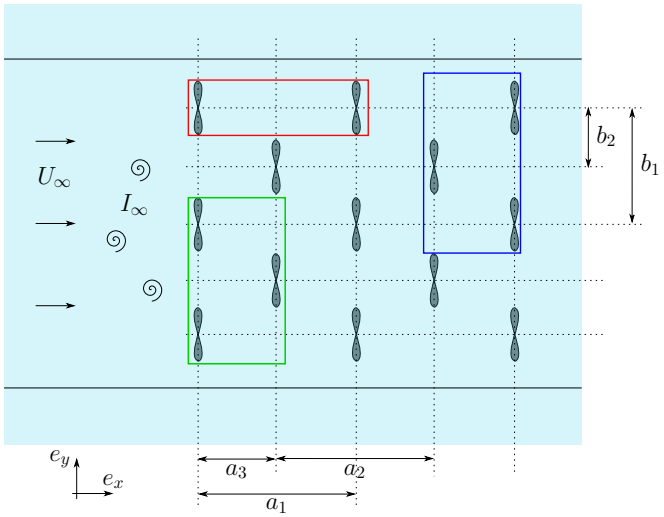

Fig. 1. Marine current turbines array with example of elementary interactions.

II. Numerical method

The software developed to compute marine current turbines [6] is based on the Vortex method [7]–[9]. This method is an unsteady Lagrangian method where the flow is discretised using vorticity carrying particles. And the turbines are represented using a panel method [10]. At first, general outlines of the Vortex Method will be presented. Then, in a second phase, the numerical development carried out to reduce the computational cost for simulation with several turbines will be detailed.

A. Vortex Method

The Navier-Stokes equations for an unsteady and incompressible flow are used in their velocity/vorticity $(\vec{u}, \vec{\omega})$

formulation:

$$\nabla \cdot \overrightarrow{\boldsymbol{u}} = 0, \tag{1}$$

$$\frac{D\overrightarrow{\boldsymbol{\omega}}}{Dt} = \left(\overrightarrow{\boldsymbol{\omega}} \cdot \nabla\right) \overrightarrow{\boldsymbol{u}} + \nu \Delta \overrightarrow{\boldsymbol{\omega}}, \tag{2}$$

where $\overrightarrow{\boldsymbol{u}}$ is the velocity field, $\overrightarrow{\boldsymbol{\omega}} = \nabla \wedge \overrightarrow{\boldsymbol{u}}$ is the vorticity field and ν is the kinematic viscosity. Equation (2) basically represents the momentum equation in the velocity-vorticty formulation. $\left(\overrightarrow{\boldsymbol{\omega}} \cdot \nabla\right) \overrightarrow{\boldsymbol{u}}$ stands for the stretching term and $\nu \Delta \overrightarrow{\boldsymbol{\omega}}$ for diffusion. Thanks to viscous splitting (see Chap. 5 of Cottet & Koumoutsakos [9]), diffusion is handled via a Particle Strength Exchange model initially developed by Degond & Mas-Gallic [11] and Choquin & Huberson [12]. Additionally, an LES model with a turbulent eddy viscosity based on the work of Mansour *et al.* [13] completes the numerical model for diffusion. One can refer to [6] for more detailed information.

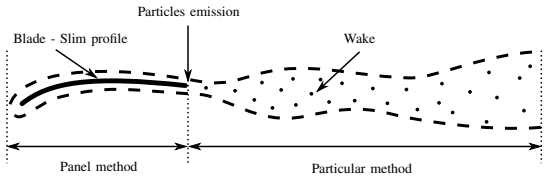

Fig. 2. Decomposition of the Vortex method.

The Helmholtz decomposition of the velocity field (eq. (3)) is used in order to decompose the velocity vector:

$$\overrightarrow{\boldsymbol{u}} = \nabla \wedge \overrightarrow{\boldsymbol{\psi}} + \nabla\phi + \overrightarrow{\boldsymbol{u}}^{\infty} = \overrightarrow{\boldsymbol{u}}^{\psi} + \overrightarrow{\boldsymbol{u}}^{\phi} + \overrightarrow{\boldsymbol{u}}^{\infty}. \tag{3}$$

Thus the velocity field is divided into three parts:

- a potential component $\overrightarrow{\boldsymbol{u}}^{\phi}$ representing the influence of the turbines blades on the flow (see Fig. 2). This component $\overrightarrow{\boldsymbol{u}}^{\phi}$ of the velocity field is obtained using a panel method [10] to solve

  $$\Delta\phi = 0. \tag{4}$$

  Equation (4) is obtained by introducing equation (3) in the continuity equation (eq. (1)). Evaluation of this potential velocity may lead to some increases in term of computational cost for multiple turbines computations. Sub-section II-C details more precisely the developed computational techniques in order to cope with this difficulty.
- a rotational component $\overrightarrow{\boldsymbol{u}}^{\psi}$ representing the wake of the turbines (see Fig. 2). The component $\overrightarrow{\boldsymbol{u}}^{\psi}$ is the solution of the equation

  $$\Delta\overrightarrow{\boldsymbol{\psi}} = -\overrightarrow{\boldsymbol{\omega}}, \tag{5}$$

  obtained by introducing the Helmholtz decomposition (eq. (3)) in the vorticity definition $\overrightarrow{\boldsymbol{\omega}} = \nabla \wedge \overrightarrow{\boldsymbol{u}}$ [6].
- a constant vector $\overrightarrow{\boldsymbol{u}}^{\infty}$ representing the upstream tidal current. The upstream velocity can be modified as presented in ref. [14] in order to take into account for ambient turbulence.

In order to make the link between the rotational and the potential parts of the velocity, particles are emitted at the trailing edge thanks to a Kutta-Joukowski condition [6], [15], [16]. The emitted particles are then advected in the flow as shown in Fig. 2. The emission scheme was recently modified in order to take into account more precisely the blades' feet influence on the near wake of the turbine. Thanks to those modifications an improvement of the near wake (≤ 4 diameters) representation was achieved.

As for the potential part $\overrightarrow{\boldsymbol{u}}^{\phi}$ of the velocity, representing the influence of the turbines, it is obtained by using a distribution of normal dipoles on the turbines surface S. In order to achieve that, the turbine is divided into N_P surface elements. Each of those elements is defined by its centre P, its normal vector $\overrightarrow{\boldsymbol{n}}(P)$, its surface ds_P and μ_P its normal dipole supposed constant on the surface element. Thus, the velocity $\overrightarrow{\boldsymbol{u}}^{\phi}$ can be expressed on each point M as the sum of the contribution of each surface element P_j:

$$\overrightarrow{\boldsymbol{u}}^{\phi}(M) = \frac{1}{4\pi} \sum_{j=1}^{N_P} \mu_{P_j} \nabla_M \left(\frac{\overrightarrow{\boldsymbol{MP_j}} \cdot \overrightarrow{\boldsymbol{n}}(P_j)}{|\overrightarrow{\boldsymbol{MP_j}}|^3} \right) ds_{P_j}. \tag{6}$$

The dipole distribution is obtained at each time step thanks to a slip condition at the centre P of each surface element. This slip condition imposes a normal velocity equal to zero in the mobile frame of the blade:

$$\overrightarrow{\boldsymbol{u}}(P_j) \cdot \overrightarrow{\boldsymbol{n}}(P_j) = \overrightarrow{\boldsymbol{u}}^{\Omega}(P_j) \cdot \overrightarrow{\boldsymbol{n}}(P_j) \quad \forall j \in [\![1, N_P]\!], \tag{7}$$

where $\overrightarrow{\boldsymbol{u}}^{\Omega}(P_j)$ represents the velocity induced at the centre of the surface element j by the rotation of the blade. This slip condition (7) on each surface element leads to the resolution of the linear system (8). The linear system (8) is a matrix system of size N_P and needs to be solved at each time step:

$$A\overrightarrow{\boldsymbol{\mu}} = \overrightarrow{\boldsymbol{b}}, \tag{8}$$

where the matrix A is call *influence matrix* and its components A_{ij} are:

$$A_{ij} = \left(\frac{1}{4\pi} \nabla_{P_i} \left(\frac{\overrightarrow{\boldsymbol{P_iP_j}} \cdot \overrightarrow{\boldsymbol{n}}(P_j)}{|\overrightarrow{\boldsymbol{P_iP_j}}|^3} \right) ds_{P_j} \right) \cdot \overrightarrow{\boldsymbol{n}}(P_i) \quad \forall i, j \in [\![1, N_P]\!]. \tag{9}$$

The i^{th} elements of $\overrightarrow{\boldsymbol{b}}$, the right hand side of eq. (8) is basically the translation of the free slip condition (eq. (7))

$$b_i = -\left(\overrightarrow{\boldsymbol{u}}^{\infty}(P_i) + \overrightarrow{\boldsymbol{u}}^{\psi}(P_i) - \overrightarrow{\boldsymbol{u}}^{\Omega}(P_i)\right) \cdot \overrightarrow{\boldsymbol{n}}(P_i) \quad \forall i \in [\![1, N_P]\!], \tag{10}$$

B. Turbine description and geometrical parameters

The turbines used in this study are anti-clockwise three bladed horizontal axis turbines. The turbines blades are designed from a NACA63418 profile. More details about the blades geometry are given in Pinon *et al.* [6]. An example of the mesh used in numerical simulation is shown in Figure 3. The different parameters describing the mesh are:

- dh the inter-particle spacing;

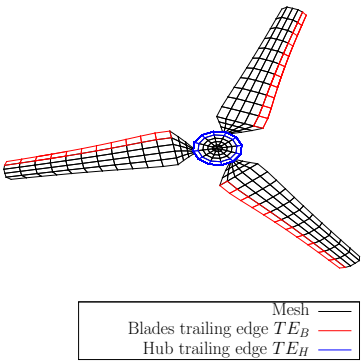

Fig. 3. Description of the mesh

- N_{TE_B} the number of element representing a blade trailing edge (red in Figure 3);
- N_{TE_H} the number of element representing the hub trailing edge (blue in Figure 3);
- ϵ the smoothing parameter which is proportional to dh:

$$\epsilon = 1.5 \times dh. \tag{11}$$

The ϵ smoothing parameter is used in order to desingularise the Biot & Savart equation, solving equation (5) and not presented here. The reader can refer to ref. [6] for clarification. The different parameters values describing the meshes are presented in Table I.

dh	N_{TE_B}	N_{TE_H}	ϵ	N_P
0.158	5	6	0.236	488
0.113	7	8	0.169	641
0.072	11	12	0.107	964
0.053	15	16	0.079	1278
0.034	23	24	0.051	1914

TABLE I
DESCRIPTION OF THE DIFFERENT MESH PARAMETERS.

C. Case of interacting turbines

The linear system (8) has to be solved at each time step. In the case of computation with a single turbine, the matrix A is constant. Indeed the definition of its components A_{ij} (eq. (9)) is only geometrical. And as the turbine geometry is supposed constant over time, therefore the matrix A is constant over time as shown in Fig. 4. The influence matrix being constant, its inverse matrix A^{-1} can be evaluated at the beginning of the computation, stored and re-used at each time step. This configuration only costs a single matrix-vector multiplication per time step, which is not critical.

Unfortunately the situation becomes more complicated for simulations with several machines. In fact, as shown in Fig. 5, the influence matrix A is modified at each time step as the relative position between turbines changes over time (relation 5 (green) in Fig. 5). Therefore, the linear system (8) needs to be fully resolved at each time step. Matrix inversion being unaffordable for large turbines array configuration, an iterative method was then chosen to solve the system with a more reasonable computational cost.

In order to solve this linear system (8) efficiently, different iterative methods were tested: a Jacobi method, a basic Conjugate Gradient (CG) and a Bi-Conjugate Gradient Stabilized (Bi-CGSTAB). The influence matrix A being neither symmetrical nor positive-definite nor diagonally dominant, the Bi-CGSTAB method [17] was the only method which assures the solution convergence for such matrices. The matrices being close to symmetry, close to diagonal dominance and with only very few negative eigen values, the other methods were however tested.

Table II depicts convergence comparison of different iterative methods in the case of a configuration with 4 turbines for different mesh sizes dh (see Table I of Sub-section II-B). The integer values stand for the number of iteration i required for the leftover $|Ax_i - b|/|b|$ to reach the machine precision ($\approx 2.2 \cdot 10^{-16}$). If the method needs more than 500 iterations to reach that precision, then the leftover value is displayed in parenthesis. As assumed, and now further validated by the results presented in Table II, the Bi-CGSTAB method is the only one to converge whereas the two other methods hardly achieve a leftover of 10^{-2} after 500 iterations.

Moreover, it is well known that an appropriate preconditioning can highly reduce the number of iterations necessary to obtain the convergence of an iterative method. A basic Jacobi preconditioning was first tested without much success (see Table II). One of the most noticeable property of the influence matrix A is that the diagonal blocks represent the influence between two panels of the same turbine (relation 1 to 4 in Fig. 5). Thus in the case of n interacting turbines, the matrix A has a natural n constant diagonal blocks property and only the non-diagonal blocks change over time. Taking advantage of this property, a block-Jacobi preconditioner is also used in order to speed-up the Bi-CGSTAB method (see Table II). One can clearly observe that only 3 iterations per time step are now required with this preconditioning. Conjugate Gradient methods with a block-Jacobi preconditioner also performs well with only 5 iterations per time step. The Conjugate Gradient algorithm being less CPU time consuming, this alternative could have being chosen as a more effective solution. However, convergence is not mathematically proven for our matrices so the conservative solution of block-Jacobi preconditioning Bi-CGSTAB algorithm was finally chosen. A complete and detailed description regarding this aspect of the method is under preparation for future publication. However, this new block-Jacobi preconditioned Bi-CGSTAB method really speeds up the computation. And it offers the possibility of multi-turbines configurations, even for fine discretisations of the turbines. Some examples of multi-turbines configurations will be presented in the following section IV.

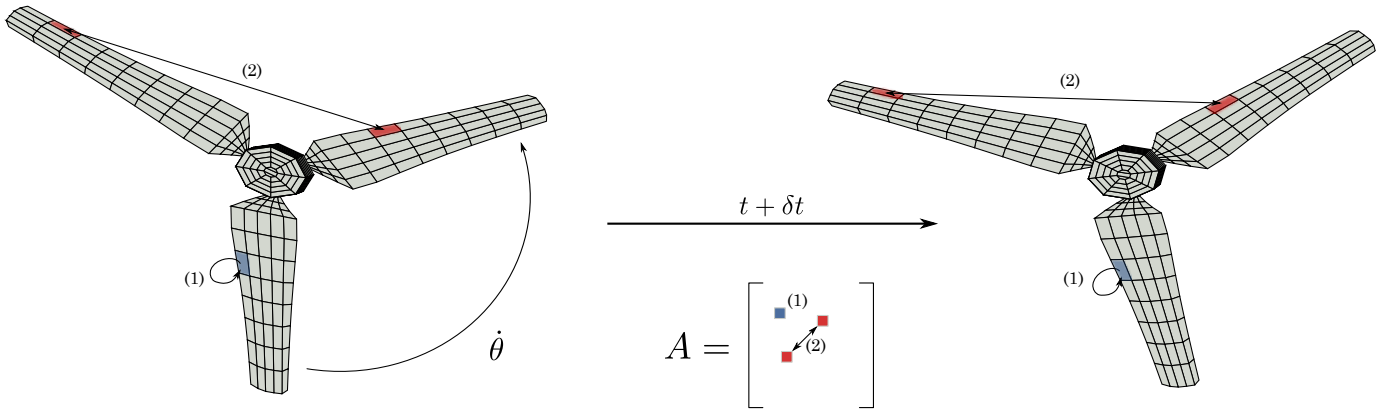

Fig. 4. Influence matrix construction in the case of a single turbine.

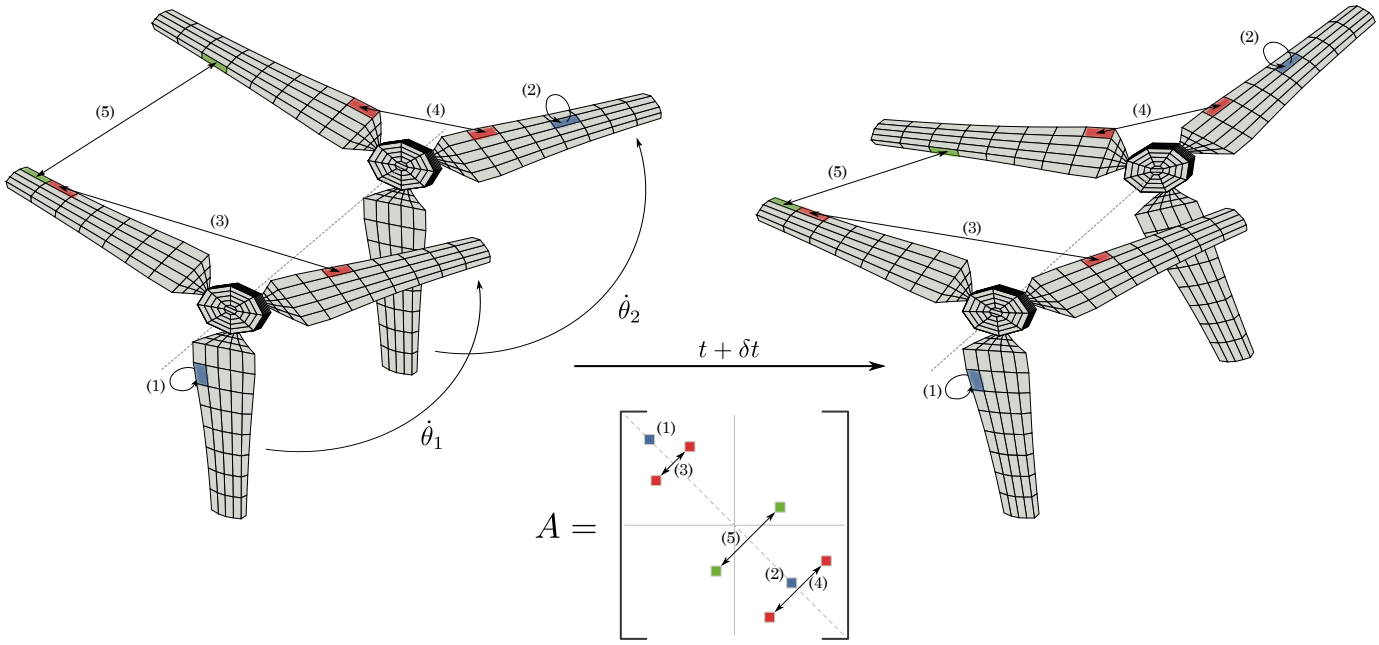

Fig. 5. Influence matrix construction in the case of a two interacting turbines.

III. Experimental study

A. Experimental setup

The experimental set-up used at the IFREMER flume tank of Boulogne-sur-Mer (France) is described in Fig 6 and much more details are available in ref. [18] and [19]. The main experimental parameters used during those trials are:

- the upstream velocity $U_\infty = |\overrightarrow{\boldsymbol{u}}^\infty|$,
- the ambient turbulence intensity I_∞

$$I_\infty = 100\sqrt{\frac{\frac{1}{3}[\sigma^2(u_\infty)+\sigma^2(v_\infty)+\sigma^2(w_\infty)]}{\bar{u}_\infty^2+\bar{v}_\infty^2+\bar{w}_\infty^2}}, \quad (12)$$

  whose values are set either to $I_\infty = 3\%$ or 15%.
- the Tip Speed Ratio (TSR)

$$\mathrm{TSR} = \frac{\Omega_x R}{U_\infty}, \quad (13)$$

  where $R = D/2$ stands for the radius of the turbine model and Ω_x stands for its rotation speed.

The experimental trials were performed using three bladed horizontal axis turbines regulated in rotation speed. The three experimental models of turbine had a $0.70\,m$ diameter, which corresponds to a scale of around $1/25^{th}$ and Reynolds number range from 1.4×10^5 to 4.2×10^5. The Reynolds number is based on the turbine radius R, the free stream velocity U_∞ and the kinematic viscosity ν. The turbines performances are measured thanks to a load cell and a torque sensor (see Fig 6). Hence the performances are determined by the calculation of power coefficient C_P and trust coefficient C_T:

$$C_P = \frac{\mathcal{M}_x \Omega_x}{\frac{1}{2}\rho\pi R^2 U_\infty^3}, \quad (14)$$

$$C_T = \frac{\mathcal{F}_x}{\frac{1}{2}\rho\pi R^2 U_\infty^2}, \quad (15)$$

with $\mathcal{M}_x$ the axial moment (or torque), defined as the x-component moment (x being the upstream current direction),

	Without preconditioning			Jacobi preconditioning		Jacobi by blocs preconditioning	
dh	Jacobi	CG	Bi-CGSTAB	CG	Bi-CGSTAB	CG	Bi-CGSTAB
0.158	(10^{-2})	(10^{-2})	194	(10^{0})	94	5	3
0.113	(10^{-2})	(10^{-2})	193	(10^{-2})	123	5	3
0.072	(10^{-1})	(10^{1})	269	(10^{1})	150	5	3
0.053	(10^{-1})	(10^{1})	301	(10^{0})	164	5	3
0.034	(10^{-1})	(10^{0})	288	(10^{9})	143	5	3

TABLE II

CONVERGENCE COMPARISON OF DIFFERENT ITERATIVE METHOD IN THE CASE OF A CONFIGURATION WITH 4 TURBINES FOR DIFFERENT MESH SIZES dh. THE INTEGER VALUES STAND FOR THE NUMBER OF ITERATION i NEEDED FOR THE LEFTOVER $|Ax_i - b|/|b|$ TO REACH THE MACHINE PRECISION ($\approx 2.2 \cdot 10^{-16}$). IF THE METHOD NEEDS MORE THAN 500 ITERATIONS TO REACH THAT PRECISION THEN THE LEFTOVER ORDER OF VALUE IS DISPLAYED IN PARENTHESIS.

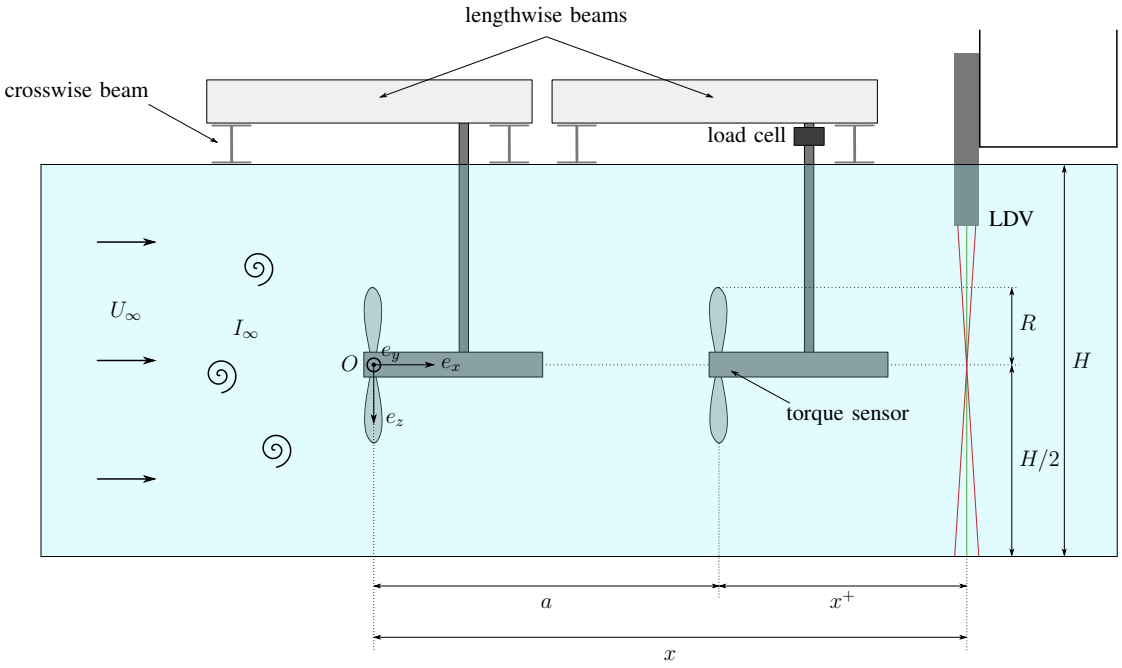

Fig. 6. Schematic view of the experimental setup for the case of two interacting turbines aligned with the upstream current (red in Fig. 1).

ρ the fluid density and $\mathcal{F}_x$ the axial force on the whole turbine (including the blades, hub and mast). As for the wake measurements, a two components Laser Doppler Velocimetry (LDV) system was used. The present study aims to numerically reproduce the elementary interaction effects obtained experimentally between two or three turbines. On the contrary to [14], the paper will not take into account the effects of the ambient turbulence and for that reason, only the experimental results obtained with the lower turbulence intensity (*i.e.* $I_\infty = 3\%$) will be considered. The experimental results used in this paper for numerical/experimental validation are those of Mycek *et al.* [19] for the configuration with two aligned turbines and those of Kervella *et al.* [5] for the configurations with three turbines.

B. Experimental results

The first elementary interaction presented here is the case of two aligned turbines with the flow as presented by the red box in Figure 1. This corresponds to the simplest but most critical interaction possible as the wake of the upstream turbine directly hits the second turbine. Figure 7 displays the wake velocity maps downstream of a single turbine and downstream of a second turbine with all the same Tip Speed Ration (TSR $= 3.67$). This experimental comparison of velocity maps shows strong differences between the two wakes. Indeed the velocity deficit is more important in the near wake ($x^{+*} \leq 2$) for the second turbine configuration than in the case of a single turbine. This can be explained by the fact that the flow has absolutely not recovered its infinite velocity $\overrightarrow{\boldsymbol{u}}^\infty$ at the location of the second turbine, indicated by the black line of Figure 7(a). On the contrary, the velocity recover in the far wake ($x^{+*} \geq 4$) is better in the wake of a second turbine than in the case of a single machine.

Thus, the wake of the downstream turbine dissipates more quickly than the one of a single turbine. The encountered phenomenon is complex because vortical coherent structures issuing from the wake of the upstream turbine combined with wake generated turbulence increase the overall turbulence

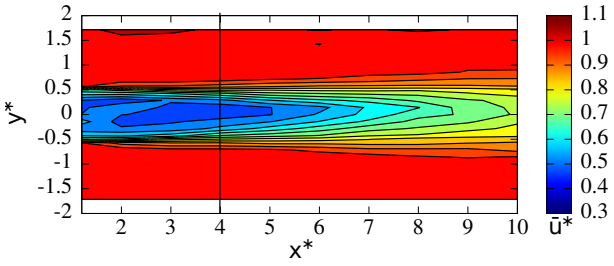

(a) Single turbine velocity map

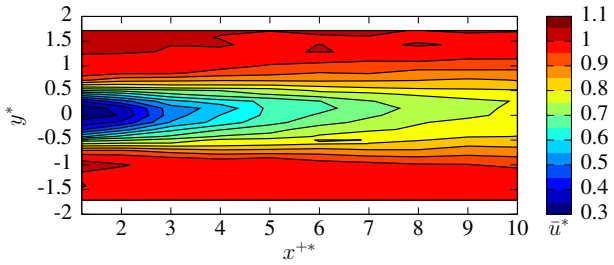

(b) Downstream turbine velocity map

Fig. 7. (a) Wake velocity map of a single turbine and (b) wake velocity map of the downstream turbine for two aligned turbines configuration with inter-device distance of $a_1 = 4D$ as presented on the schematic representation of Figure 1. The other parameters are $U_\infty = 0.8m.s^{-1}$ and $\mathrm{TSR}^{single} = \mathrm{TSR}^{up} = \mathrm{TSR}^{down} = 3.67$. $x^* = x/D$, $y^* = y/D$ and x^{+*} corresponds to a non dimensional downstream position from the second turbine $x^* = a_1/D + x^{+*}$.

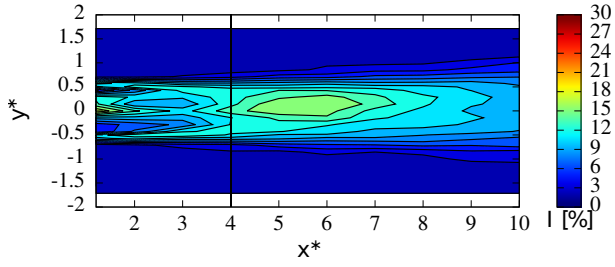

(a) Single turbine turbulence intensity map

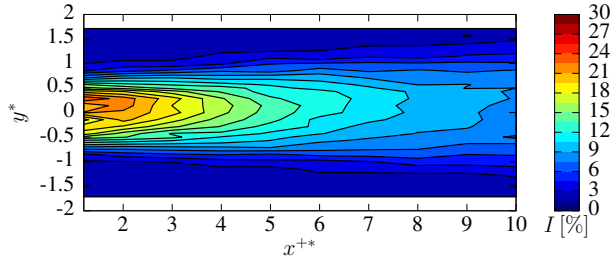

(b) Downstream turbine turbulence intensity map

Fig. 8. (a) Turbulence intensity map in the wake of a single turbine and (b) turbulence intensity map in the wake of the downstream turbine for two aligned turbines configuration with inter-device distance of $a_1 = 4D$ as presented on the schematic representation of Figure 1. The other parameters are $U_\infty = 0.8m.s^{-1}$ and $\mathrm{TSR}^{single} = \mathrm{TSR}^{up} = \mathrm{TSR}^{down} = 3.67$. $x^* = x/D$, $y^* = y/D$ and x^{+*} corresponds to a non dimensional downstream position from the second turbine $x^* = a_1/D + x^{+*}$.

intensity at the location of the downstream turbine, indicated by the black line of Figure 8(a). The turbulence intensity level at this location is around 12% to be compared with the ambient turbulence $I_\infty = 3\%$ of the upstream flow. A higher wake dissipation for higher ambient turbulence I_∞ was already highlighted in previous studies [18] but the case of two aligned turbines is much more complex. Some evidences of that can be observed on the power coefficient C_P of the downstream turbine, whose determination is not trivial. However, a detailed study on the second turbine efficiency is presented in ref. [19] based on experimental results. Some experimental/numerical cross validation on this configuration were already presented using the same numerical tool [4] and some improvements on this results are going to be presented and discussed in the following section together with new numerical results on three turbines configurations.

IV. Numerical study

A. The case of two aligned turbines

As mentioned earlier, this configuration of elementary interaction is critical if ones want to accurately compute performances of turbines arrays. In order to validate the performance assessment of the second device in such a configuration, a ratio r_{C_P} (eq. (16)) between the downstream device performance $C_P^{down}(\mathrm{TSR})$ with respect to the single turbine performance $C_P^{single}(\mathrm{TSR}) = C_P^{up}(\mathrm{TSR})$ is calculated either experimentally or numerically. A similar ratio r_{C_T} (eq. (17)) is evaluated for thrust coefficient C_T:

$$r_{C_P}(\mathrm{TSR}) = \frac{C_P^{down}(\mathrm{TSR})}{C_P^{up}(\mathrm{TSR})} \tag{16}$$

$$r_{C_T}(\mathrm{TSR}) = \frac{C_T^{down}(\mathrm{TSR})}{C_T^{up}(\mathrm{TSR})}. \tag{17}$$

These two ratios evaluate the proportion of a single turbine performance attained by the downstream turbine. Figure 9 presents numerical and experimental values of these ratios as a function of the inter-devices distance a_1/D. First, the two experimental curves (for $\mathrm{TSR} = 3$ and 4) show that these two ratios grow with the inter-devices distance a_1/D. As expected, this growth proves that the more distance between turbines, the better the second turbine performances are. But those experimental results also show that even for large distances between the two devices, the downstream turbine performances are highly reduced. For instance, for the given turbulence intensity of $I_\infty = 3\%$, the power coefficient C_P of the downstream turbine only attains around 80% of the single turbine performance for an inter-device distance a_1 of 10 diameters (D). Thus, there is a loss in performance of 20% for the second turbine even $10D$ behind. These experimental results, as well as some others, are well presented and discussed in Mycek *et al.* [19].

Secondly, Figure 9 also presents the numerically predicted values together with the experimental ones. The computations were run using a discretisation $dh = 0.072$ of Table I for an overall computations of $24\,s$ for the configuration with 4 diameters inter-devices distance to $32\,s$ for the 8 diameters

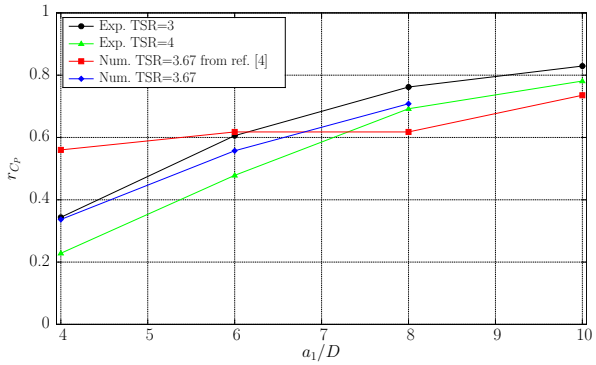

(a) r_{C_P}

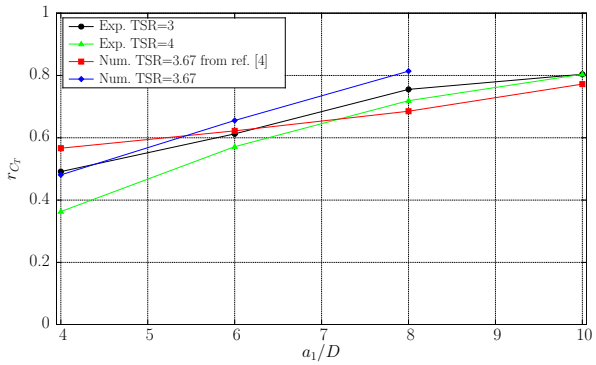

(b) r_{C_T}

Fig. 9. Numerical and experimental comparison of C_P and C_T ratio of equations (16) and (17) for a given $\mathrm{TSR} = \mathrm{TSR}^{up} = \mathrm{TSR}^{down}$ indicated in the legend. Most experimental results were reproduced from ref. [19] and the former numerical results from ref. [4].

one. The presented values are the average values of the last $4\,s$ of the overall computation.

The presented results shows a rather good agreement between experimentally and numerically predicted values. Indeed, the blue curve in Figure 9 represents the recent values of r_{C_P} and r_{C_T} obtained thanks to the latest development on the particles emission scheme. These new values have a better agreement with the experiments than those previously presented by Mycek *et al.* [4] (red in Figure 9). This improvement in the numerical result is especially noticeable when the two turbines are close (*i.e.* $a_1 = 4D$; and $a_1 = 6D$ to a smaller extent). The results presented in Figure 9 tend to give a good confidence in the numerical tool to represent the negative interactions effects on the performance of the second turbine. However, work is also under progress in order to assess these ratios for other TSR in order to have accurate values for different inter-device spacing and different TSR.

Additionally, the ambient turbulence plays an important role for such a simple configuration (see ref. [19]), for that reason, similar computations with different ambient turbulences I_∞ are already planned following the work of Carlier *et al.* [14]. And finally, a systematic study of wake assessment, even for the downstream turbine, is planned the near future in order to compare with the existing experimental database. So far as wakes are considered, the following sub-section will present wake computations for three turbines configurations similarly to the experimental results of Kervella *et al.* [5].

B. Interactions between three turbines

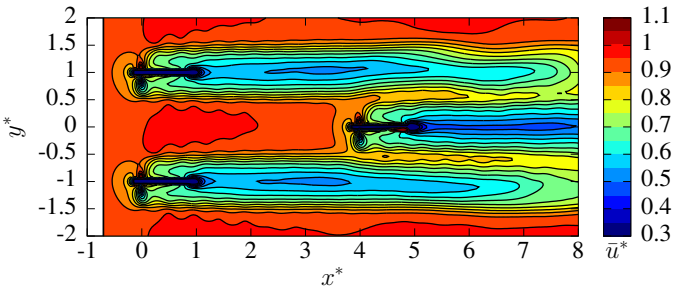

Fig. 10. Numerical wake for the configuration 2 (green in Figure 1) at $TSR = 2$ for the three turbines configurations. The inter-device distances are defined so that $a_3 = 4D$ and $b_1 = 2 * b_2 = 1D$ with respect to the scheme of Figure 1.

Figures 10 and 11 depict instantaneous velocity fields for three turbines configurations inspired from the experimental work of Kervella *et al.* [5]. These two configurations complete the possible elementary interactions presented in Figure 1 as they refer to the green and blue boxes. The inter-device distances are defined so that $a_3 = 4D$ and $b_1 = 2 * b_2 = 2D$. These instantaneous velocity fields correspond to $t \approx 28.2\,s$. The computations were run using a discretisation $dh = 0.158$ of Table I for 399 unsteady iterations of time $dt = 0.07066\,s$. The presented results actually do not really match with the experiments of Kervella *et al.* [5] in terms of TSR values. Additionally, as they correspond to the coarsest mesh discretisation, improvement in the quality of the result are expected in a near future. However, these results are already very interesting qualitatively as many physical aspects are already observable even for these discretisations, like the wake interaction clearly visible on both Figures 10 and 11 as soon as the wake of the first row of turbine(s) reaches the second row.

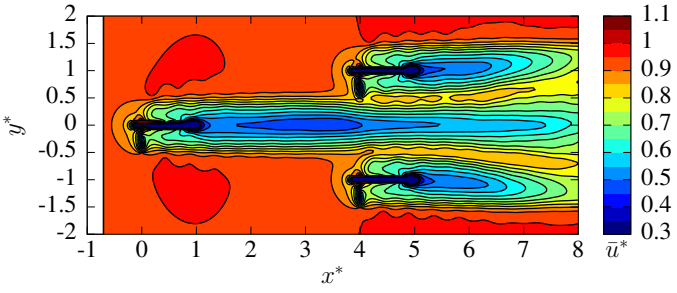

Fig. 11. Numerical wake for the configuration 3 (blue in Figure 1) at $TSR = 2$ for the three turbines configurations. The inter-device distances are defined so that $a_3 = 4D$ and $b_1 = 2 * b_2 = 1D$ with respect to the scheme of Figure 1.

V. Conclusions and Further works

The three dimensional software [6] developed at LOMC in partnership with IFREMER was used in order to compute

elementary interactions between tidal turbines. Recent numerical developments carried out to reduce the computational cost of simulations with several turbines were presented. The choice of the preconditioned Bi-CGSTAB method to solve the linear system during simulation with multiple turbines was first presented and justified.

As a matter of results, this paper presents studies of elementary interactions between two or three turbines. The study of two aligned turbines have shown that the performance of the downstream turbine is highly reduced, especially in the case of low ambient turbulence. Indeed, the power coefficient C_P of the downstream turbine still presents a 20% loss with respect to a single turbine, even for an inter-device distance a_1 of 10 diameters. Many more details of these interaction effects, obtained experimentally, are presented in Mycek *et al.* [19].

The present study mainly focuses on numerical computations of these elementary interactions. First, the case of two aligned turbines was computed in terms of performance analysis. This study highlights the improvement of the numerical results achieved thanks to the recent development on the particles emission scheme, with respect to a previous attempt [4]. Preliminary results on the case of three turbines, similarly to the configuration of Kervella *et al.* [5], are also presented in terms of wake velocity maps. These test cases gave accurate results when compared to the experiments and computations of arrays with several turbines are close to be accessible. However, the ambient turbulence plays an important role (see for instance ref. [19]). For that reason, similar computations with different ambient turbulences I_∞ are already planned following the work Carlier *et al.* [14]. And finally, a systematic study of performances and wake assessment is planned in the near future in order to compare with the existing experimental database of two and three turbines interaction for the two accessible turbulence intensities (*i.e.* $I_\infty = 3\%$ and $I_\infty = 15\%$).

ACKNOWLEDGMENT

The authors would like to thank Haute-Normandie Regional Council and Institut Carnot IFREMER Edrome for their financial supports for C. Carlier Ph.D. Grant and "GRR Energie" programs. The authors also would like to thank the CRIHAN (Centre des Ressources Informatiques de Haute-Normandie) for their available numerical computation resources.

REFERENCES

[1] R. Malki, I. Masters, A. Williams, and T. Croft, "The influence on tidal stream turbine spacing on performance," in *9th European Wave and Tidal Energy Conference (EWTEC)*, September 2011, Southampton, UK.

[2] D. O'Doherty, A. Mason-Jones, C. Morris, T. O'Doherty, C. Byrne, P. Prickett, and R. Grosvenor, "Interactions of marine turbines in close proximity," in *9th European Wave and Tidal Energy Conference (EWTEC)*, September 2011, Southampton, UK.

[3] L. Myers and A. Bahaj, "An experimental investigation simulating flow effects in first generation marine current energy converter arrays," *Renewable Energy*, vol. 37, no. 1, pp. 28–36, 2012. [Online]. Available: http://www.sciencedirect.com/science/article/pii/S0960148111001716

[4] P. Mycek, B. Gaurier, G. Germain, G. Pinon, and E. Rivoalen, "Numerical and experimental study of the interaction between two marine current turbines," *International Journal of Marine Energy*, vol. 1, no. 0, pp. 70 – 83, 2013. [Online]. Available: http://www.sciencedirect.com/science/article/pii/S2214166913000088

[5] Y. Kervella, G. Germain, B. Gaurier, J.-V. Facq, and T. Bacchetti, "Mise en évidence de l'importance de la turbulence aambiant sur les effets d'interaction entre hydroliennes," in *XIIIèmes Journées Nationales Génie Côtier – Génie Civil*, 2014.

[6] G. Pinon, P. Mycek, G. Germain, and E. Rivoalen, "Numerical simulation of the wake of marine current turbines with a particle method," *Renewable Energy*, vol. 46, no. 0, pp. 111 – 126, 2012. [Online]. Available: http://www.sciencedirect.com/science/article/pii/S0960148112002418

[7] C. Rehbach, "Calcul numérique d'écoulements tridimensionnels instationnaires avec nappes tourbillonaires," *La Recherche Aérospatiale*, vol. 5, pp. 289–298, 1977.

[8] R. Lewis, *Vortex element methods for fluid dynamic analysis of engineering systems*. Cambridge University Press, 1991.

[9] G. Cottet and P. Koumoutsakos, *Vortex methods: theory and practice*. Cambridge University Press, 2000.

[10] J. Bousquet, *Méthode des singularités*. Cépaduès - Editions, 1990.

[11] P. Degond and S. Mas-Gallic, "The weighted particle method for convection-diffusion equations. Part I: The case of an isotropic viscosity," *Math. Comp.*, vol. 53, no. 188, pp. 485–507, 1989. [Online]. Available: http://dx.doi.org/10.2307/2008716

[12] J. Choquin and S. Huberson, "Particles simulation of viscous flow," *Computers & Fluids*, vol. 17, no. 2, pp. 397 – 410, 1989. [Online]. Available: http://www.sciencedirect.com/science/article/pii/0045793089900492

[13] N. Mansour, J. Ferziger, and W. Reynolds, "Large-eddy simulation of a turbulent mixing layer," Report TF-11, Thermosciences Div., Dept. of Mech. Eng., Stanford University, Tech. Rep., 1978.

[14] C. Carlier, G. Pinon, B. Gaurier, G. Germain, and Élie Rivoalen, "A synthetic-eddy-method to represent the ambient turbulence in numerical simulation of marine current turbine," in *11th European Wave and Tidal Energy Conference (EWTEC)*, September 2015, Nante, France.

[15] F. Hauville and Y. Roux, "Réglage dynamique d'une voile par une méthode d'intéraction fluide/structure," in *9èmes Journées de l'Hydrodynamique*, 2003.

[16] P. Mycek, "étude numérique et expérimentale du comportement d'hydroliennes," Ph.D. dissertation, Université du Havre, 2013.

[17] H. A. van der Vorst, "Bi-CGSTAB: a fast and smoothly converging variant of Bi-CG for the solution of nonsymmetric linear systems," *SIAM J. Sci. Statist. Comput.*, vol. 13, no. 2, pp. 631–644, 1992. [Online]. Available: http://dx.doi.org/10.1137/0913035

[18] P. Mycek, B. Gaurier, G. Germain, G. Pinon, and E. Rivoalen, "Experimental study of the turbulence intensity effects on marine current turbines behaviour. part I: One single turbine," *Renewable Energy*, vol. 66, no. 0, pp. 729 – 746, 2014. [Online]. Available: http://www.sciencedirect.com/science/article/pii/S096014811400007X

[19] ——, "Experimental study of the turbulence intensity effects on marine current turbines behaviour. part II: Two interacting turbines," *Renewable Energy*, vol. 68, no. 0, pp. 876 – 892, 2014. [Online]. Available: http://www.sciencedirect.com/science/article/pii/S0960148114000196